An Ultraweak Focusing Proton EDM Storage Ring

Richard Talman
Laboratory for Elementary-Particle Physics
Cornell University

October 3, 2017

Abstract

A "weak/weaker, alternating-gradient, combined-function" (WW-AG-CF) electric storage ring is described. It is optimized for an experiment proposed to measure the proton electric dipole moment (EDM). The main bending field exists in the tall slender gaps between inner and outer, vertically-plane, horizontally-curved electrodes. The full ring consists of repetitions of such sector bends separated by drifts, correctors, RF cavities and so on.

Between cylindrical (curved-planar) electrodes, the radial electric field dependence is $E_r \sim 1/r^{1+m}$, where the field index m is exactly $m = 0$. This field produces horizontal bending as well as horizontal "geometric" focusing but, because the field provides no vertical force, some vertical focusing has to be incorporated to prevent particles from escaping vertically. The design described here provides this focusing by "alternating gradient" (not quite flat) electrode contouring, with m toggling from sector to sector, for example, between $m = -0.002$ and $m = +0.002$. Alternating focusing and defocusing provides net focusing. But this is not "strong-focusing". It is "weak-weaker" focusing, just barely strong enough to keep particles captured. The resulting beam distributions are highly asymmetric, much higher than they are wide. This matches the good field storage ring aperture. Other than the electrode shaping (present only in regions of almost-exactly-magic velocity), and weak, ideally zero strength correctors, *there are no quadrupoles,* which is favorable for systematic error reduction.

The pure $m = 0$ field is also advantageous from the point of view of (complete absence of) spin decoherence. This advantage is sacrificed by adjusting m away from zero but, to leading order, this decoherence cancels for the proposed symmetrically positive and negative deviations of m.

Another important consideration concerns intrabeam scattering (IBS), which is potentially the most serious source of run-duration-limiting emittance growth. The proposed desigh stabilizes the ring against IBS by permitting adjustment (in the lattice design stage) for "below transition" ring operation.

Contents

1 Introduction

Measuring the proton electric dipole moment (EDM) with best possible precision requires an electrostatic storage ring in which 233 MeV, frozen spin polarized protons can be stored for an hour or longer without depolarization. Initially single beams would be stored, with run-to-run alternation of circulation directions. For ultimate reduction of systematic error, simultaneously counter-circulating beams would be stored.

For longest spin coherence time (SCT), and to best exploit the systematic error reduction enabled by counter-circulating beams, the focusing needs to be as weak as possible, and the beam energy spread as small as possible. The lattice proposed here to meet these requirements is (to construct an acronym) of WW-AG-CF, "weak-weaker, alternating-gradient, combined-function" type. (Not counting trim quadrupoles) there are no quadrupoles. The entire vertical focusing is provided by alternating gradient, horizontally-curved electrodes. Because the required vertical focusing is so weak it may be possible for the electrodes to be completely flat vertically, with unbalanced electrical powering, along with slight vertical element shifts providing the focusing. In any case, to the naked eye, the electrodes would appear to be essentially flat. The horizontal bending is designed to be on a circle, or rather circular arcs, of radius $r_0 = 40\,\mathrm{m}$.

If the vertical field shaping is produced electrically it could provide zero quadrupole focusing. This would allow stabilization of the vertical plane by octupole focusing. However this possibility is not addessed in the present paper—only conventional, combined-function focusing is considered.

To stabilize the beam against intrabeam scattering (IBS) emittance dilution it is considered essential for the lattice to run "below transition"; i.e. where the orbital period is more influenced by change in velocity than by change in momentum. The proposed design meets this requirement. The next section is largely devoted to demonstrating this behavior, by first calculating the dispersion. For the ultraweak focusing that is optimal for the EDM measuement the focusing associated with electrical (in contrast with magnetic) bending is especially important.

The subsequent section contains lattice functions for a first-pass-optimized lattice. Following that is a formal treatment of betatron oscillations in an all-electric lattice. As well as being needed for operational control of the ring, this material is intended to be applied later to decoherence calculations that are, as yet, incomplete.

2 Orbits for "cylindrical" ($E_r \approx 1/r$) electric field

2.1 The pure cylindrical case

Much of this paper has been extracted from references[1],[2], and [3]. As shown in Figure 1, in cylindrical (r, θ, y) coordinates, an electric field with index m power law dependence on radius r for y=0 is

$$\mathbf{E}(r,0) = -E_0 \frac{r_0^{1+m}}{r^{1+m}} \hat{\mathbf{r}}, \tag{1}$$

and the electric potential $V(r)$, adjusted to vanish at $r = r_0$, is

$$V(r) = -\frac{E_0 r_0}{m}\left(\frac{r_0^m}{r^m} - 1\right). \tag{2}$$

Strictly speaking this dependence applies only in the horizontal design plane. And yet it is

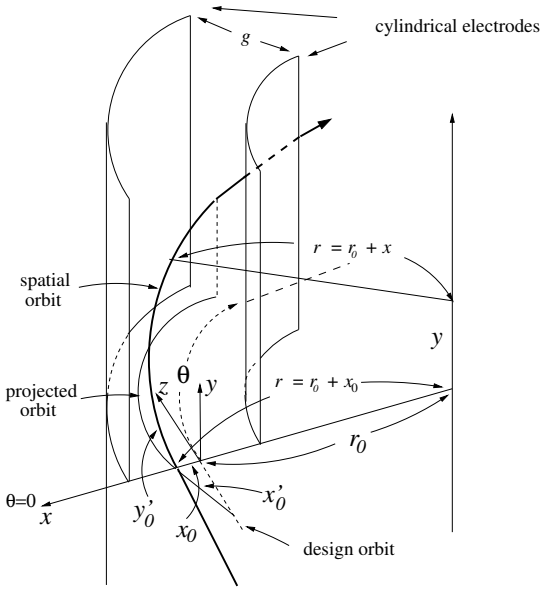

Figure 1: The bold curve shows a proton orbit passing through a curved-planar cylindrical electrostatic bending element. The electrode spacing is g and the design orbit is centered between the electrodes.

vertical focusing in which we are primarily interested.

The horizontal focusing is dominated by geometric focusing which makes no contribution to vertical focusing. We start by calculating the excess horizontal focusing caused by the tailoring of the power law dependence by vertical shaping of the pole pieces. For designing this tailoring we are treating the electrodes as longitudinally straight, rather than toroidal, which is their actual shape. Though not strictly correct, this can be a satisfactory approximation if the sector angles are quite short. This is especially valid for horizontal focusing, because it is primarily geometric. The *total vertical focusing* is equal in magnitude, but opposite in sign, to the *horizontal focusing deviation* caused by the pole shaping. The vertical focusing is therefore being calculated only approximately, but with better validity as the bend sector lengths are reduced. Eventually the full three dimensional fields will have to be calculated correctly.

For m=1, inverse square-law dependence, the field can be referred to as "Kepler" or as "Coulomb", though the treatment now has to be fully relativistic. The relativistic Kepler problem can be solved with the same closed-form generality in the relativistic as in the non-relativistic case; however the orbits are neither exactly elliptical, nor closed.

We are more concerned with the "cylindrical" case shown in Fig. 1; curved-planar electrodes produce an electric field, for which m=0. For $m = 0$ there is "geometric" focusing of

an on-momentum particle corresponding to its global circular orbit. For m positive the electric field strength decreases with increasing r, which causes an on-momentum particle with x positive to be turned less strongly—i.e. weakening the horizontal focusing. Associated with this there is correspondingly-weak vertical *focusing*. At least some vertical focusing will be required. This can easily be provided with separated function quadrupoles, but there is a reason it is better to provide the necessary vertical focusing by choosing $m \neq 0$. The reason, as demonstrated below, is that *the magic velocity condition is orders of magnitude more accurately met in bend regions than in drift regions.* Actually, rather than simple weak focusing, it is proposed here to have "alternating gradient" focusing by alternating $m < 0$ and $m > 0$ bend sectors.

The task is to determine general orbits, such as the bold curve in the figure. Using the customary local Frenet (x, y) coordinates, its initial radial displacement (from the design orbit) and its radial slope are x_0 and x_0'. The initial vertical slope is y_0'. Any particular orbit will also have some initial vertical displacement y_0. For m=0, y_0 can be set to zero without loss of generality, since the apparatus then has vertical translational symmetry. This paper emphasizes cases in which m is small enough for this invariance to be at least approximately true. At some point, though, it will be necessary to accept the fact that the idealization of the electrodes as being vertical infinite, as well as being experimentally impossible, can, without care, lead to theoretical contradictions (for example when vertical element misalignment is being considered)

The orbit is also influenced by the proton's initial fractional total (mechanical plus potential) energy deviation from nominal, $\Delta\mathcal{E} = \mathcal{E} - \mathcal{E}_0$. This makes, altogether, four independent initial conditions. Unlike in a magnetic field, the magnitude of the momentum is *not* conserved in the electric bends. Given initial conditions $X(\theta = 0) = \big(x_0, x_0', y_0'; \Delta\mathcal{E}_0\big)$, the task is to solve for $X(\theta) = \big(x(\theta), x'(\theta), y(\theta), y'(\theta), \Delta\mathcal{E}_0\big)$. Note, here, that the fourth component does not change—with potential energy included in the definition of total energy, $\mathcal{E}$ *is conserved*. But the mechanical energy, conveniently represented as $\gamma m_p c^2$, is not conserved in general. Only the sum of mechanical and potential energy is conserved. On entering or exiting a bending element it is necessary to account for the changes in potential energy.

The central, or design, orbit is a circle of radius r_0, midway between the circular cylinder electrodes of radii $r_0 \pm g/2$. Defining the (inward-directed) electric field on the central orbit as (positive) E_0, for the cylindrical, $m = 0$ case, the field is given by[1]

$$\mathbf{E}(r, \theta, y) = -E_0 \, \frac{r_0}{r} \, \hat{\mathbf{r}}. \tag{3}$$

The electric potential $V(r)$, adjusted to vanish on the design orbit, is

$$V(r) = E_0 r_0 \ln \frac{r}{r_0} = E_0 r_0 \ln r - E_0 r_0 \ln r_0. \tag{4}$$

[1]We are using r as a cylindrical coordinate, even though, as used in Eq. (3), r is more conventionally taken to be a polar coordinate, which would make the field exactly central, irrespective of the value of m. For y=0, polar and cylindrical coordinates are identical and, at least in an accelerator, because the ring radius is large compared to Δr, cylindrical and spherical r-coordinates are usually nearly indistinguishable.

The "magic" kinematic parameters satisfy

$$\gamma_0 = \sqrt{\frac{g}{g-2}} = \sqrt{1+\frac{1}{G}}, \tag{5}$$

where G is the "anomalous magnetic moment" and $g = 2G + 2$. (Occasionally the symbol "a" is used instead of the symbol "G".) For the proton EDM experiment this yields the following kinematic quantities for frozen proton spin operation:

$$\begin{aligned} c &= 2.99792458e8\,\mathrm{m/s} \\ m_p c^2 &= 0.93827231\,\mathrm{GeV} \\ G &= 1.7928474 \\ g = 2G+2 &= 5.5856948 \\ \gamma_0 &= 1.248107349 \\ \mathcal{E} = \gamma_0 m_p c^2 &= 1.171064565\,\mathrm{GeV} \\ K0 = \mathcal{E} - m_p c^2 &= 0.232792255\,\mathrm{GeV} \\ p0c &= 0.7007405278\,\mathrm{GeV} \\ \beta_0 &= 0.5983790721 \end{aligned} \tag{6}$$

2.2 Coordinate transformation: $x \rightarrow \xi = x/r$

The kinematic values just given are fixed by the "frozen-spin" requirement of the experiment. For examples in this paper, $r_0 = 40.0\,\mathrm{m}$. The design parameters are then related by Newton's centripetal force law

$$eE_0 r_0 \left(\frac{r_0}{r}\right)^{1+m} = \frac{\beta_0 p_0 c}{r} \overset{\text{also}}{=} \frac{m_p c^2}{r}\left(\gamma_0 - \frac{1}{\gamma_0}\right), \tag{7}$$

where r_0 is design radius and r is the radius of an arc of a circle with the same center, and where p, v, and β are proton momentum, velocity, and v/c. These equalities are specific to circular orbits, with γ_0 applying to the design orbit. If γ_0 should have the magic value of 1.248107349 the equalities apply to frozen spin proton operation. On the design orbit the electric potential is defined to be zero, both inside, on the circular orbit and ouside, on the adjacent tangential field-free drifts. For the pure cylindrical case with $m = 0$, because the factor r can be cancelled from all three expressions, one has the singular result that, independent of radius, all circular orbits have the same speed. One cannot, for example, solve Eqs. (7) to find the radius of an off-momentum circular orbit.

For approximately cylindrical electric fields with non-vanishing m-values, rather than using transverse coordinate $x = r - r_0$, it is convenient to introduce a variable $\xi = x/r$, which satisfies the relations

$$\xi = \frac{x}{r} = \frac{x}{r_0 + x} = 1 - \frac{r_0}{r}, \quad r = \frac{r_0}{1-\xi}. \tag{8}$$

Expressed in terms of ξ, the electric field at radius r is given by

$$\mathbf{E}(\xi) = -E_0\,(1-\xi)^{1+m}\,\hat{\mathbf{r}}, \tag{9}$$

Consider a nearby "parallel", circular/straight-line orbit having radius $r = r_0 + x$ inside a bend, with tangential straight line orbits displaced by x outside. The relativistic gamma factor on the orbit (inside) is γ^I, which satisfies

$$eE_0 r_0\,(1-\xi)^m = \beta^I p^I c = m_p c^2\Big(\gamma^I - \frac{1}{\gamma^I}\Big), \tag{10}$$

On this orbit, for $r \neq r_0$, because of the change in electric potential at the boundary, the gamma factor outside has a different value, γ^O.

For $m \neq 0$ the orbit determination is no longer degenerate. Expressing Eq.(10) as a quadratic equation for γ^I, the coefficient of the term linear in γ^I is $-E_0 r_0(1-\xi)^m/(m_p c^2/e)$, and the gamma factor for a circular orbit at radius r is given by the positive root;

$$\gamma^I(\xi) = \frac{E_0 r_0(1-\xi)^m}{2m_p c^2/e} + \sqrt{\left(\frac{E_0 r_0(1-\xi)^m}{2m_p c^2/e}\right)^2 + 1}. \tag{11}$$

This function is plotted in Figure 2 for $m = \pm 0.2$. For small m the slopes $d\gamma^I(\xi)/d\xi$ are proportional to m. By designing an "alternating gradient", "combined function' (AG-CF) lattice it should be possible to arrange for the appropriately-averaged speed within bend elements of off-momentum closed orbits to be exactly "magic", even including end effects. Even in the absence of synchrotron oscillation averaging, this would cancel the spin decoherence associated with proton beam momentum spread. (The same cancelation would applly for each of two counter-circulating beams, though lattice and injection errors can cause their central values to deviate differently from magic.) Spin decoherence associated with betatron oscillations needs to be discussed separately.

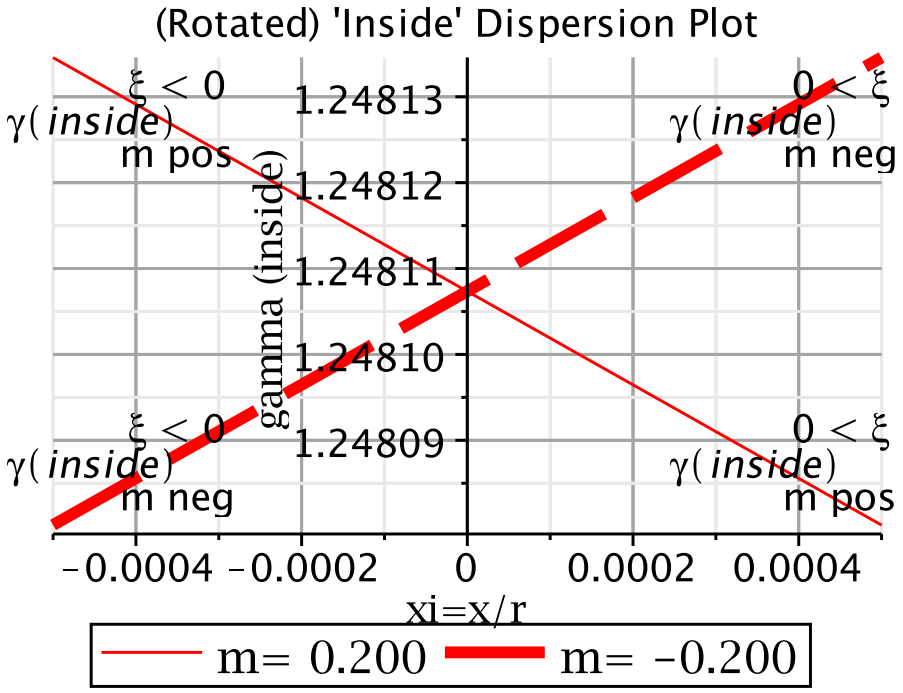

Figure 2: This figure shows a "dispersion plot" of "inside" gamma value γ^I plotted vs ξ. The curves intersect at the magic value $\gamma^I = 1.248107$. Because $d\gamma/d\beta = \beta\gamma^3$ is equal to about 1.17 at the magic proton momentum, the fractional spreads in velocity, momentum, and gamma are all comparable in value—in this case about $\pm 2 \times 10^{-5}$. This figure may be confusing, since it is rotated by 90 degrees relative to conventional dispersion plots. For this reason one should also study the following plot, which is identical except for being rotated, and is annotated as an aid to comprehension. Subsequent plots have the present orientation, however.

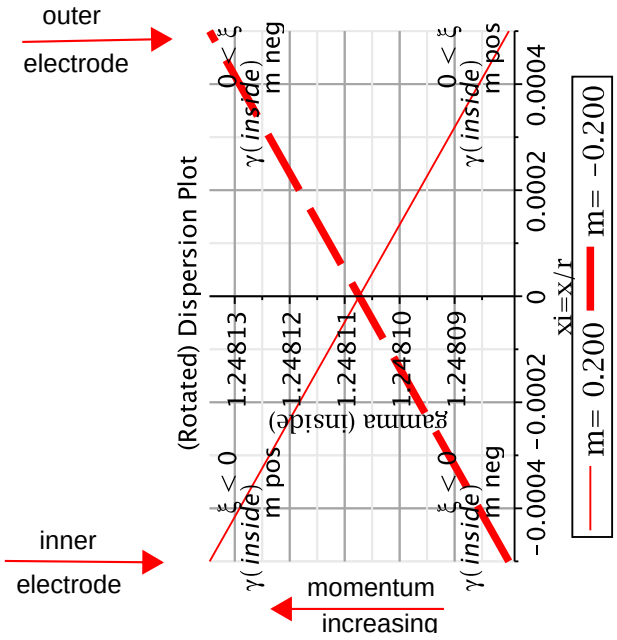

Figure 3: This plot is identical to the previous one except for being rotated by 90 degrees into conventional orientation (except momentum increases from right to left). It shows the dependence of $\xi = x/r$ vs "inside" gamma value γ^I, for $m = -0.2$ and $m = 0.2$. Note that, for $m < 0$ larger momentum causes larger radius while, for $m > 0$ the opposite is true. *What is striking is that the slope is opposite for* $m > 0$ *and* $m < 0$. *This is "anomalous".*

It is important to appreciate that, from the point of view of spin decoherence, the average particle speeds in drift sections need not be independent of momentum. This is because there is no spin precession in drift sections, so no spin decoherence would result. Furthermore, the ring is not necessarily "isochronous"; i.e. the mean revolution period does not need to be independent of momentum offset. Still, the dependence of revolution period on momentum offset can be expected to be very small, and the synchrotron oscillation frequency correspondingly small, and not necessarily favorable as regards being above or below transition. Quantifying this issue is one of the goals of the present analysis. For these reasons it is important to calculate velocities exactly in drift sections.

A possible alternating-gradient, combined-function, AG-CF storage ring can be formed from elements described by the fixed m-value curves shown in Figure 2, by alternating the m-values of the bending elements making up the ring. Toward understanding such a ring, it is instructive to apply energy conservation to match "gamma-inside" γ^I curves to obtain matching γ^O values.

Expressed as power series in ξ, with the leading terms cancelling, the electric potential is given by

$$\begin{aligned} V(r) &= -\frac{E_0 r_0}{m}\left((1-\xi)^m - 1\right) \\ &= E_0 r_0\left(\xi + \frac{1-m}{2}\xi^2 + \frac{(1-m)(2-m)}{6}\xi^3 \ldots\right). \end{aligned} \tag{12}$$

This simplifies spectacularly for the Kepler m=1 case. But we are concerned with the small $|m| << 1$ case.

As a proton orbit passes at right angles from outside to inside a bend element, its total energy is conserved;

$$\begin{aligned} \gamma^O(\xi) &= \frac{\mathcal{E}^O}{m_p c^2} = \frac{\mathcal{E}^I}{m_p c^2} \\ &= \gamma^I(\xi) + \frac{E_0 r_0}{m_p c^2/e}\left(\xi + \frac{1-m}{2}\xi^2 + \frac{(1-m)(2-m)}{6}\xi^3 \ldots\right). \end{aligned} \tag{13}$$

Plots of $\gamma^O(\xi)$ for $m = \pm 0.2$ are shown in Figure 4.

Voltages supplied to the electrodes, causing the field index values to alternate between $m = -0.2$ and $m = +0.2$, are shown schematically in Figure 5. (The semi-circular appearance of this figure is only for pictorial convenience—the bend angles of individual elements will not exceed several degrees.) The alternating m-values cancel the spin decoherence of off-momentum particles having zero betatron excitation; i.e. each exactly following its off-momentum closed orbit. The resulting evolution of extreme off-momentum closed orbits is shown Figure 6.

(In practice one may accept slighty offset orbits rather than introducing the complicated powering shown in Figure 5, and apply appropriate corrections. Whether or not this is done, we neglect the miniscule longitudinal electric fields in drift section that the weak applied correction voltages would cause.)

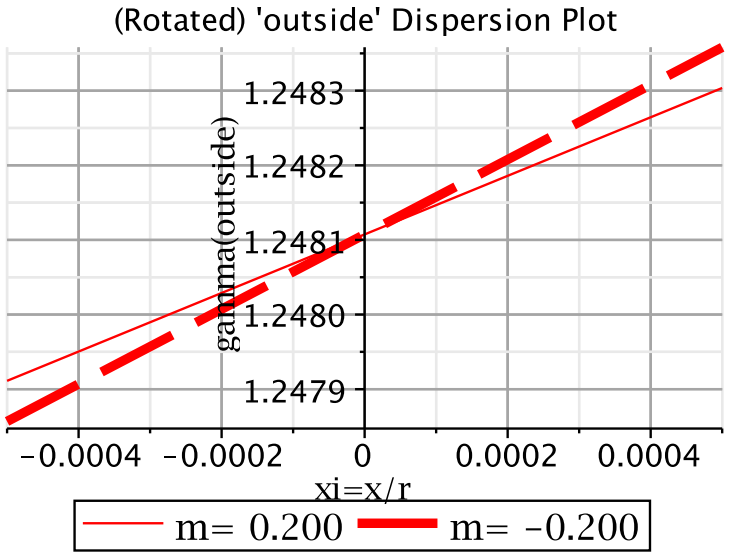

Figure 4: "Outside" dispersion plots. *Note that dispersion slopes are the same for* $m < 0$ *and* $m > 0$. Dependence of "outside" gamma value γ^O on $\xi = x/r$ for $m = -0.2$ and $m = 0.2$. Because $d\gamma/d\beta = \beta\gamma^3$ is equal to about 1.17 at the magic proton momentum, the fractional spreads in velocity, momentum, and gamma are all comparable in value—in this case about 2×10^{-4}. *The fractional spreads are an of magnitude greater outside than inside.*

2.3 Dispersion for $|m| << 1$, appoximately cylindrical, bends

There is a conventional accelerator physics formalism for defining off-energy equilibrium orbits in magnetic rings; a "dispersion function" D is defined which describes the incremental horizontal displacement accompanying an incremental change in energy, or (more conventionally) fractional momentum offset δ.

The simplest possible ring has alternating drifts and sector bends. Off-energy closed orbits continue to be circlular in bend regions, entering and exiting normal to the element ends. Because of the potential energy discontinuity at the end of a bend element it is appropriate to distinguish, by superscripts I and O, between kinematic variables respectively inside and outside bend elements. Since their x coordinates are constant through drifts, the paths of off-momentum closed orbits in consecutive bend elements just amount to continuation of the circle from the previous bend. It is not necessary to distinguish between r^I and r^O for off-momentum closed orbits, since r is continuous at the ends of bend elements.

If we were completely consistent in using the subscript I, as in γ^I, for particles inside the element, then we could afford to (but, usually, will not) drop the O, as in just γ, outside bend elements. The point is that being "outside" a magnet element and being "outside" an electric element is the same thing—so conventional formalism should carry over unchanged from magnetic to electric rings, as long as we are in free space regions (and correctly account for orbit evolution through electric elements). One simplifying fact is that, since the potential is zero by definition on the design orbit, then $\gamma = \gamma_0$ on the design orbit, whether inside or outside bend elements.

Even for a ring with no drift sections (so particles are almost always "inside") we recom-

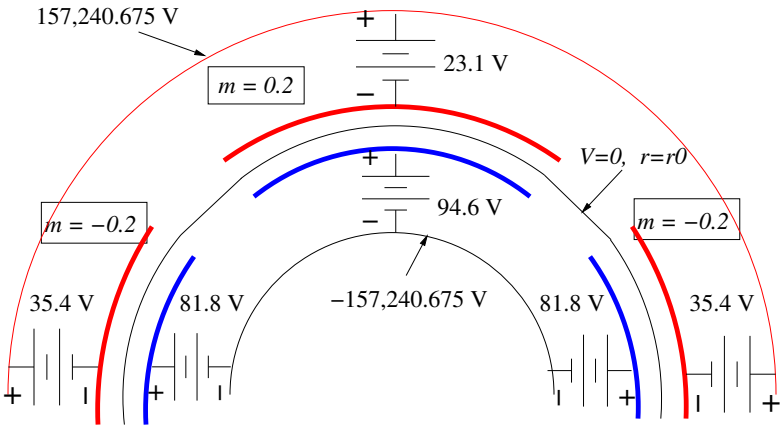

Figure 5: Schematic of voltages applied to inner and outer electrodes of alternating $m = -0.2$ and $m = 0.2$ "cylindrical" electrode bending elements to produce electric fields that exactly cancel spin decoherence among particles that are on-momentum with zero betatron oscillation amplitudes. The electrodes are perfectly circular arcs in the horizontal, design, up-down symmetry plane, separated by 3 cm (but slightly different above and below, depending on the m value). Electric fields vanish in the drift sections between the bend elements, except for tiny longitudinal fields off-axis (i.e. $E_z \neq 0$ for $x \neq 0$).

mend using γ^O to differentiate individual particles (for example in RF cavities) whether the particle is inside or outside. [2]

From Eq. (7), with cylindrical electrodes, $m = 0$, the linearized dependence of off-momentum closed orbit displacement (circular arc) on fractional momentum offset is given by

$$r = \frac{1}{eE_0/c}\,\beta^I p^I \stackrel{\text{also}}{=} r_0 + D^I \delta^I, \tag{14}$$

where D^I is the "dispersion inside" and $\delta^I = (p^I - p_0)/p_0$ is the fractional momentum offset inside. Kinematically

$$\left.\frac{d(\beta^I p^I)}{dp^I}\right|_{r_0} = \beta_0(2 - \beta_0^2). \tag{15}$$

Differentiating Eq. (14),

$$\left.\frac{dr}{dp^I}\right|_{r_0} = \frac{1}{eE_0/c}\,\beta_0(2 - \beta_0^2) \stackrel{\text{also}}{=} D^I\,\frac{1}{p_0}. \tag{16}$$

From this we obtain the dispersion inside;

$$D^I = r_0(2 - \beta_0^2). \tag{17}$$

[2] These issues are not entirely academic, since the closest thing to a "nominal" EDM lattice assumes cylindrical electrodes, which give precisely the logarithmic potential behavior and large values of dispersion under discussion. Injection into such a lattice may present problems. To avoid mismatch it seems as if the injected proton beam must have energy and transverse displacement correlated exactly as required by the dispersion function. It seems unavoidable that finite energy spread at fixed displacement ("slice emittance" would be the phrase used for beams in bunch compressors) will lead to magnified horizontal betatron oscillations. i.e. horizontal emittance growth after filamentation. This will place a premium on achieving extremely small energy spread, perhaps by pre-cooling of some kind.

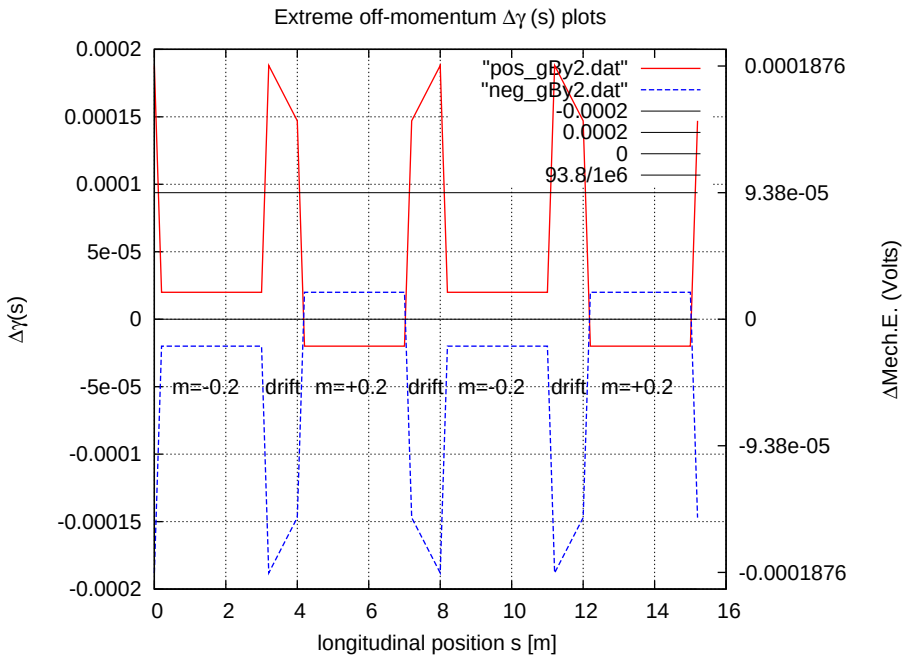

Figure 6: Dependence of deviation from "magic" $\Delta\gamma(s) = \gamma(s) - \gamma_0$ on longitudinal position s, for off-momentum closed orbits (circular arcs within bends) just touching inner or outer electrodes at $x = \pm 0.015\,\mathrm{m}$. The right hand tic labels express (approximately) the same quantities as $\Delta\gamma(s) m_p c^2/e$ mechanical energy offset values. The horizontal axis is artificial and the drift lengths arbitrary—later the drift lengths will be adjusted for below transition operation. There is no MDM spin precession in drifts and MDM spin precession in $m = 0.2$ and $m = -0.2$ exactly cancel (or could be tuned to cancel spin precession including contributions from fringe field regions.

For some purposes, especially for analysing injection and extraction, as well as synchrotron oscillations, it is the external dispersion D^O that is needed. One has

$$D^O \delta^O = D^I \delta^I. \tag{18}$$

This equality follows from the fact that, for circular orbits, the radial component $r = r_0 + x$ is conserved at bend entrances and exits. Knowing D^I, we therefore need only calculate the ratio δ^O/δ^I.

Inside and outside gamma values are related by

$$\gamma^I = \gamma^O - \frac{eE_0 x}{m_p c^2}, \tag{19}$$

reflecting the loss of kinetic energy in "climbing" from zero potential energy outside to a

higher potential energy inside. Expressed in terms of fractional momentum offset,

$$\gamma^O = \frac{\sqrt{p_0^2(1+\delta^O)^2c^2 + m_p^2c^4}}{m_pc^2} \approx \gamma_0\sqrt{1 + \frac{2p_0^2c^2\delta^O}{\gamma_0^2m_p^2c^4}} \approx \gamma_0 + \frac{\gamma_0 p_0^2c^2\delta^O}{\gamma_0^2m_p^2c^4}$$

$$= \gamma_0 + \gamma_0\beta_0^2\delta^O, \quad \text{yielding} \tag{20}$$

$$\delta^O = \frac{\gamma^O - \gamma_0}{\gamma_0\beta_0^2}. \tag{21}$$

From the final equation we obtain

$$\frac{d\delta^O}{d\gamma^O} = \frac{1}{\gamma_0\beta_0^2}. \tag{22}$$

(At the magic proton velocity, $\gamma_0\beta_0^2 = 1.25 \times 0.6^2 = 0.45$, implying $\delta^O = 2.22\,\Delta\gamma^O$.)

Corresponding relations apply inside. Substitution into Eq.(18) and then (17) produces

$$D^O = D^I\frac{\delta^I}{\delta^O} = \left(r_0(2-\beta_0^2)\right)\frac{\gamma^I - \gamma_0}{\gamma^O - \gamma_0}. \tag{23}$$

Figures 2 and 4 have shown that, depending on the sign of m, it is not unusual for the "inside" and "outside" dispersions to have opposite sign. For positive m the slopes in Figures 2 and 4 are opposite, which seems counter-intuitive—for positive dispersion (which is normal) further out orbits have larger momentum. Positive m behaviour can therefore be referred to as "anomalous"—farther out orbits have smaller momentum. This reversal at $m = 0$ provides justification for having referred to the perfect cylindrical electrode case as "singular". Though Eq. (23) has been derived assuming $m = 0$, one sees from Figure 6 that the outside dispersion D^O varies just enough through drift sections to match the different D^I values in adjacent bends. One therefore expects the dispersion in a lattice for which m alternates, say between -0.2 and 0.2, will be midway between the the extreme curves shown in Figure 6.

Furthermore, from Figure 6 one sees, for small m values, that $|D^I| << |D^O|$. This is a highly beneficial feature in that it allows an injected beam with (relatively) large momentum spread to match ultra-small momentum spread within electric bend elements (which is the only place where spin precession occurs).

This feature can be exploited to reduce spin decoherence greatly. In fact, as indicated in the caption to Figure 6, by alternating the sign of m, the decoherence of off-momentum (but betatron-free) orbits can be exactly cancelled, even without the benefit of synchrotron oscillation averaging.

For a ring with total length of all drift sections short compared to $2\pi r_0$, because the velocities within bends are so accurately equal, the dominant time slippage per revolution comes from the increase in radius with increasing momentum offset δ. In this sense the ring would be said to be operating "above transition". For electrode gap half-spacing $g/2 \overset{\text{say}}{=} 0.015\,\text{m}$ the orbit circumferences range from $2\pi(r_0 - g/2)$ to $2\pi(r_0 + g/2)$, so the range of excess circumferences is $\pm\pi g \approx \pm 0.05\,\text{m}$. "Fixing" this will be important, because "below transition" operation is required (to stabilize intrabeam scattering).

Revolution period of off-energy orbits. In a ring consisting only of repetitions of alternating circular arcs and drifts, the revolution period of off-energy closed orbits around the ring can be calculated easily. The sum of the arc lengths is $2\pi(r_0 + x_0)$ and all velocities within bend elements are identical; $\beta_0 c$. Let $L_{\mathrm{D,tot.}}$ stand for the sum of the lengths of the drift sections. The outside speed is given by

$$\beta^O(\delta^O) = \sqrt{1 - \frac{1}{{\gamma_0^O}^2(\delta^O)}} = \sqrt{1 - \frac{1}{(\gamma_0 + \gamma_0\beta_0^2\delta^O)^2}}. \tag{24}$$

(Neglecting fringe field effects) this is valid even if accuracy higher than linear in x_0 is required. The total revolution period is then

$$cT(\delta^O) = \frac{2\pi(r_0 + D^O\delta^O)}{\beta_0} + \frac{L_{\mathrm{D,tot.}}}{\beta^O(\delta^O)}. \tag{25}$$

To limit beam growth due to intrabeam scattering (IBS) it is necessary to run "below transition". This can be accomplished by indreasing the total drift length $L_{D,\mathrm{tot.}}$ to exceed a minimum value $L_D^{\mathrm{trans.}}$ for which the off-energy revolution period is independent of (outside) momentum. Differentiating Eq. (25) and using Eq. (22), the condition to satisfy this is

$$\frac{2\pi D^O}{\beta_0} = \frac{L_D^{\mathrm{trans.}}}{\beta^{O2}}\frac{d\beta^O}{d\delta^O} = \frac{L_D^{\mathrm{trans.}}}{\beta^{O2}}\frac{d\beta^O}{d\gamma^O}\frac{d\gamma^O}{d\delta^O} = \frac{\beta_0\gamma_0^2}{\beta^{O3}\gamma^{O3}}\,L_D^{\mathrm{trans.}}. \tag{26}$$

For frozen proton spin parameters the result is

$$L_D^{\mathrm{trans.}} = 2\pi D^O\,\beta_0\gamma_0 \approx 2\pi D_0. \tag{27}$$

Since the "inside" momentum offset is so tricky and m-dependent, it seems advisable to define dispersion always with respect to "outside" momentum offset and, therefore, to suppress the "O" superscript, for example in graphs of lattice functions plotted below.

2.3.1 Vertical motion

The formalism so far has ignored vertical motion. For our favored, $|m| << 1$, cylindrical electrode case, this an excellent, but not perfect, approximation. There are two reasons why it is so good. With cylindrical electrodes there is weak vertical field so the vertical component of momentum is approximately conserved. Also, for the proton EDM experiment, the vertical beta function is huge (certainly greater than 100 m) and the vertical emittance is tiny, $\epsilon_y \approx 0.0001$ m. A typical vertical angle is therefore $\sqrt{10^{-6}} = 1$ mr, which makes the proton vertical speed nonrelativistic. The only change in vertical velocity is due to a change in the relativistic mass (which is essentially constant). It therefore provides an excellent approximation to use

$$y = y_0 + y_0' s, \tag{28}$$

to model the vertical motion within individual elements. The vertical motion has a correspondingly negligible effect on the horizontal motion.

With the m value alternating between successive bend elements, one can take advantage of combined function (CF) alternating gradient (AG) vertical focusing. This is certainly

not "strong focusing" however. As usual with AG focusing, the alternation between weak focusing and weak defocusing can provide *very* weak net focusing.

One can inquire also as to the effect of vertical motion on synchrotron oscillations. The vertical tune is expected to be very small, let us say $Q_y < 0.01$, meaning the nominal vertical betatron wavelength is greater than $100 \times 2\pi r_0$. The maximum vertical amplitude range is unlikely to exceed $\pm 5\,\mathrm{cm}$. For r_0=40 m ring radius the maximum vertical orbit angle is therefore about $\theta_y^{\max} \approx y^{\max} Q_y / r_0$ and the maximum excess circumference per turn is roughly $\pi r_0 \theta_y^2 = \pi y^{\max 2} Q_y^2 / r_0 = 2 \times 10^{-8}\,\mathrm{m}$. This clearly has only a very small effect on synchrotron oscillations.

3 Exploiting the field index hypersensitivity

The basic, pure cylindrical electric field dependence was given in Eq. (1), which is copied here with minor variations, to allow for the possibility of having alternating gradient focusing;

$$\mathbf{E}_-(r) = \mathbf{E}_-(r_0 + x) = -(1 + m_1)\, E_0 \left(\frac{r_0}{r}\right)^{1+m_2} \hat{\mathbf{r}},$$
$$\mathbf{E}_+(r) = \mathbf{E}_+(r_0 + x) = -(1 - m_2)\, E_0 \left(\frac{r_0}{r}\right)^{1-m_1} \hat{\mathbf{r}}. \qquad (29)$$

The slightly different forms, with subscrips $\pm$, designate vertically focusing and defocusing sectors. The different initial factors cause the on-axis electric fields to differ, but only slightly. It has to be realized that these are conjectured electric potential dependencies. Electrode shapes producing these dependencies *have not* actually been demonstrated.

By tilting previously-plane electrodes one can surely produce vertical electric fields and, presumeably therefore, quadrupole-like deflections close to the beam axis. By contouring the electrode shapes, the electrodes may be "saddle-shaped" with opposite sign curvature (i.e. inverse bend radius), or toroidal, with same-sign curvatures, or tall (but truncated) parallel ruled surfaces with zero vertical curvature. In all cases, for finite electrode heights, the fields will deviate strongly away from ideal dependence as position y approaches the top or bottom edges of the electrodes.

Returning to the Eq. (29) idealizations, the field shapes can be ascribed to distant point charges, with the field indices having tiny magnitude, $|m_1| << 1$ and $|m_2| << 1$, With both m_1 and m_2, say, positive, electric field $\mathbf{E}_-$ can be thought of as the field of a fractionally stronger line charge fractionally more distant; inversely, $\mathbf{E}_+$ can be though of as due to a fractionally weaker, but closer, line charge. (Unless $m_2 = -m_1$) on the circle for which $r = r_0$ the electric fields are not quite equal. Sign reversal can be visualized as charge sign reversal or of reflecting the horizontal charge position.

This means that, since the electric fields are, in fact, due to the electric potential difference between inner cylindrical electrode of radius $r_0 - g/2$ and outer electrode of radius $r_0 - g/2$, the potential differences in the two cases will have to be (slightly) different. The on-axis fields could, instead, be made unequal by making the gaps slightly different in the two cases by altering the the electrode spacing. Using the coordinate $\xi = x/r$ introduced in Eq. (8),

and copying from Eq. (12),

$$V_-(r) = (1+m_1)\,E_0 r_0 \left(\xi + \frac{1+m_2}{2}\xi^2 + \frac{(1+m_2)(2+m_2)}{6}\xi^3 \ldots\right),$$
$$V_+(r) = (1-m_2)\,E_0 r_0 \left(\xi + \frac{1-m_1}{2}\xi^2 + \frac{(1-m_1)(2-m_1)}{6}\xi^3 \ldots\right). \qquad (30)$$

By arranging for m_1 and m_2 to be equal, we will have succeeded in shaping the electrodes to perturb the horizontal focusing oppositely in adjacent bending sectors. But, as explained previously, because the *total* vertical focusing is equal (but opposite) to the horizontal focusing *deviation*, this means we will have also arranged for alternating gradient vertical focusing. Since we need only tiny vertical focusing, the corresponding change in horizontal focusing will be unimportant.

It is important that the electric potential functions given in Eqs. (30) vanish on-axis, where $\xi = 0$. But we also have to be sure that the definition of ξ varies smoothly across boundaries between bending sectors.

We now return to an earlier (cryptic) comment that the electrodes can be parallel, with zero vertical curvature, but not be vertically infinite. With infinite vertical electrodes the electric field would have to vanish and, by symmetry, there could be no vertical focusing, which would contradict Eqs. (30). Of course the electrodes cannot, in fact, be vertically infinite. They can therefore be relatively displaced vertically. Then, if displaced alternatively up and down, and powered alternatively as well, there would be vertical electric fields in the drift regions, the up-down symmetry is destroyed, and almost perfectly flat, parallel electrodes may be satisfactory.

This discussion has been academic, in the sense that it is only for convenience that one strives to retain electrode shapes that are perfectly plane vertically. In fact, in the next section indicate, by shaping the upper and lower pole edges the good-field volume can be increased appreciably.

It is quite inconvenient, but not fundamentally important, to have the design radius r_0 being different in radially-focusing and radially-defocusing sectors, or to have the angular advances per sector be different. For this paper I assume that $|m_1|$ and $|m_2|$ are small enough for these variations to be neglected. I therefore assume the design radii and the on-axis electric fields can be treated as identical, except for alternating vertical focusing.

3.1 Electrode shape plots

The paper contains discussion of "nearly flat" field shaping near the origin by altering the electrode shape. In any case this electrode shaping is likely to be dwarfed by the electrode shaping used to maximize the good field volume. This is illustrated in Figures 7 and 8. The electrode surfaces are perfect planes from y=-50 mm to +50 mm, separated by 30 mm. With end bulbs included the electrodes extend from y=-56.8 mm to +56.8 mm. Figure 8 shows that the good field region runs from y=-42 mm to +42 mm. So, with bulb correction, the good field height is reduced at each end (from the bulb-extended length) by an amount equal to half the electrode separation.

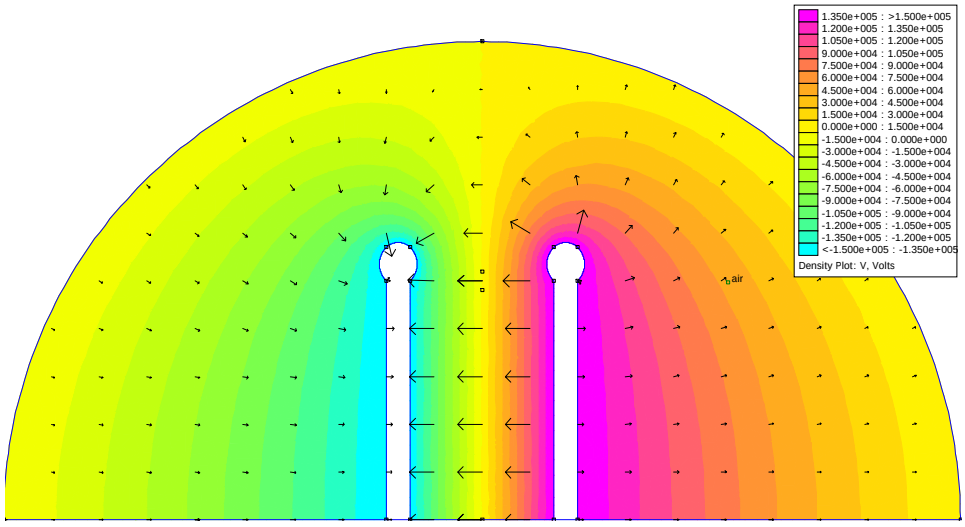

Figure 7: Electrode edge shaping to maximize uniform field volume.

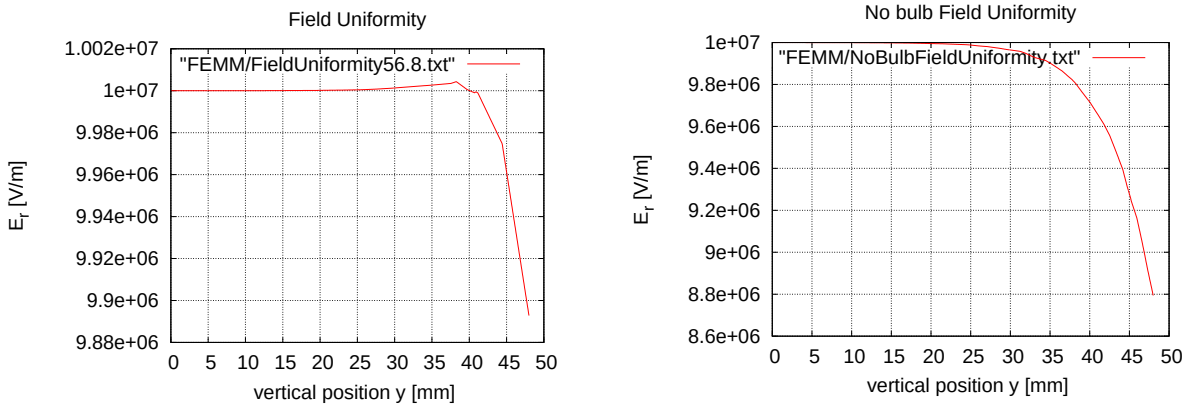

Figure 8: Plot of bulb-corrected field uniformity on the left, uncorrected on the right.

4 Lattice Functions

4.1 Parameter table

Table 1: Parameters for WW-AG-CF proton EDM lattice

parameter	symbol	unit	value
arcs			2
cells/arc	$N_{\rm cell}$		20
bend radius	r_0	m	40.0
drift length	L_D	m	4.0
circumference	$\mathcal{C}$	m	411.327
field index	m		± 0.002
horizontal beta	β_x	m	40
vertical beta	β_y	m	1620
(outside) dispersion	D_x^O	m	24
horizontal tune	Q_x		1.640
vertical tune	Q_y		0.04045
number of protons	N_p		2×10^{10}
95% horz. emittance	ϵ_x	μm	3
95% vert. emittance	ϵ_y	μm	1
(outside) mom. spread	$\Delta p^O/p_0$		$\pm 2 \times 10^{-4}$
(inside) mom. spread	$\Delta p^I/p_0$		$\pm 2 \times 10^{-7}$

4.2 Ultraweak vertical focusing adjustment

From here on ultraweak vertical focusing will be assumed. Previous plots have assumed $m = \pm 0.2$. From here on we assume $m = \pm 0.002$. Figure 9 can be compared to Figure 2 to see the greatly compressed range of "inside" γ^I that results from the reduction from $m = 0.2$ to $m = 0.002$. Since the only significant spin precession occurs in regions where the "inside" γ^I values are appropriate, this yields a huge reduction in spin decoherence.

On the other hand, the change from $m = 0.2$ to $m = 0.002$ has a much smaller effect on "outside" γ^O, as can be seen by comparing Figures 4 and 10.

4.3 Twiss function plots

Lattice functions based on the previous and subsequent formalism are plotted in Figures 11 through 16. Phase advances for both planes are plotted at all 1680 element index locations in Figure 17.

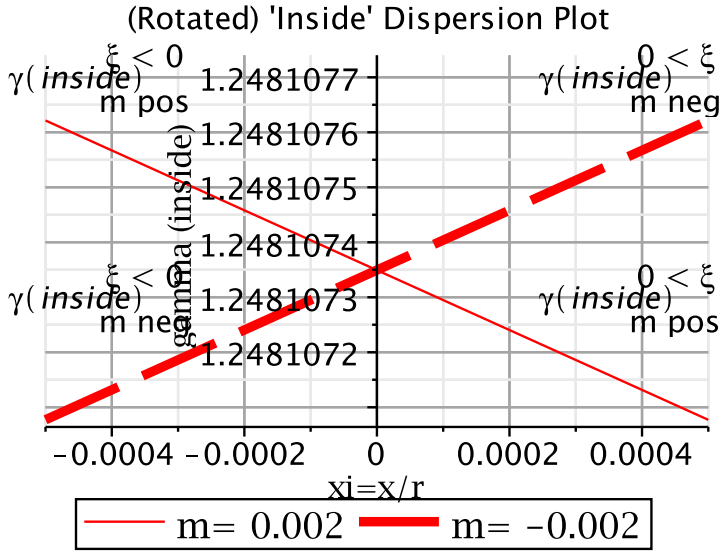

Figure 9: Dependence of "inside" gamma value γ^I on $\xi = x/r$ for $m = -0.002$ and $m = 0.002$. The curves intersect at the magic value $\gamma^I = 1.248107349$. Because $d\gamma/d\beta = \beta\gamma^3$ is equal to about 1.17 at the magic proton momentum, the fractional spreads in velocity, momentum, and gamma are all comparable in value—in this case about $\pm 3 \times 10^{-7}$—a gloriously small range.

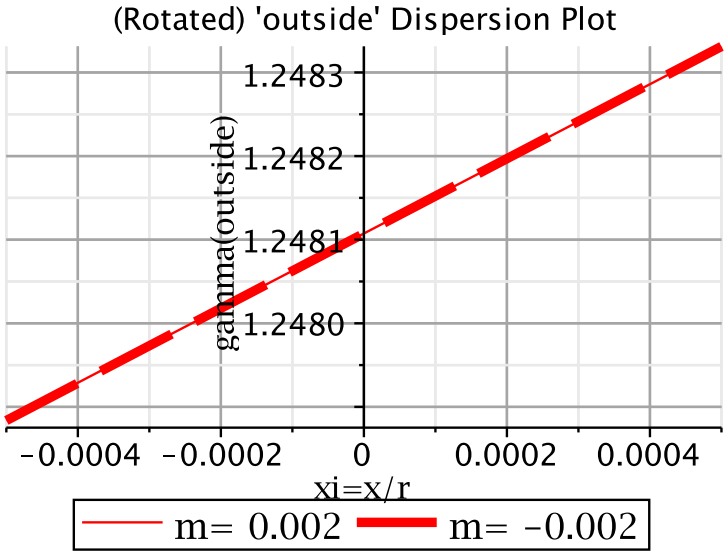

Figure 10: Dependence of "outside" gamma value γ^O on $\xi = x/r$ for $m = -0.002$ and $m = 0.002$. Because $d\gamma/d\beta = \beta\gamma^3$ is equal to about 1.17 at the magic proton momentum, the fractional spreads in velocity, momentum, and gamma are all comparable in value—in this case about $\pm 2 \times 10^{-4}$. *The fractional spreads are about three orders of magnitude greater outside than inside.*

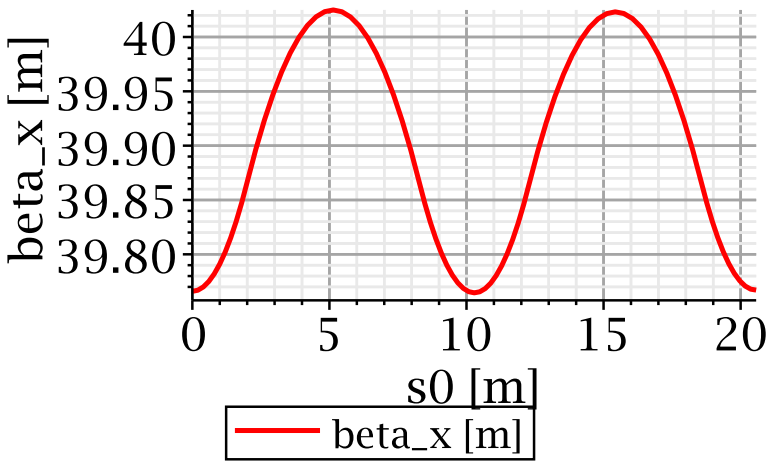

Figure 11: Horizontal beta function $\beta_x(s)$, plotted for two adjacent cells.

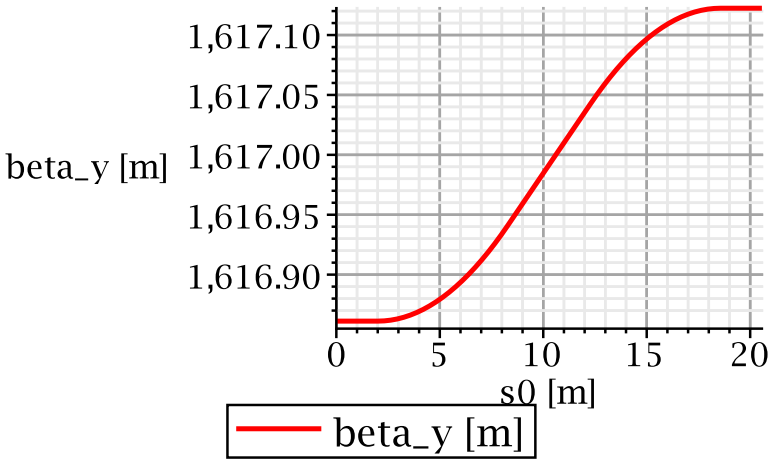

Figure 12: Vertical beta function $\beta_y(s)$, plotted for two adjacent cells. For this case the total circumference is 411.3 m and the total drift length is 160.0 m. Extended decimal places exhibit the extreme uniformity.

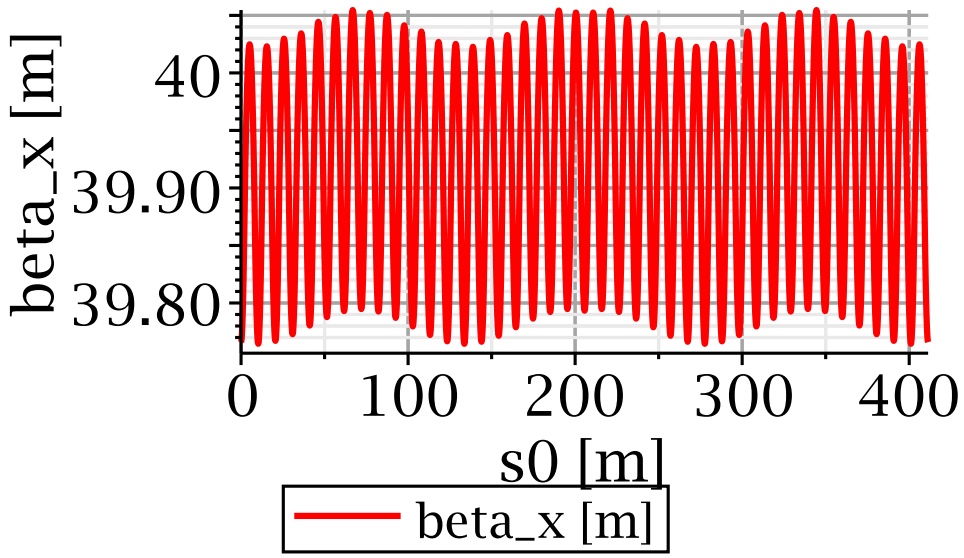

Figure 13: Horizontal beta function $\beta_x(s)$, plotted for full ring. For this case the total circumference is 411.3 m and the total drift length is L_D=160.0 m. Since this total drift length exceeds $L_D^{\text{trans.}}$ as given by Eq. (27), the ring will be "below transition", as regards synchrotron oscillations.

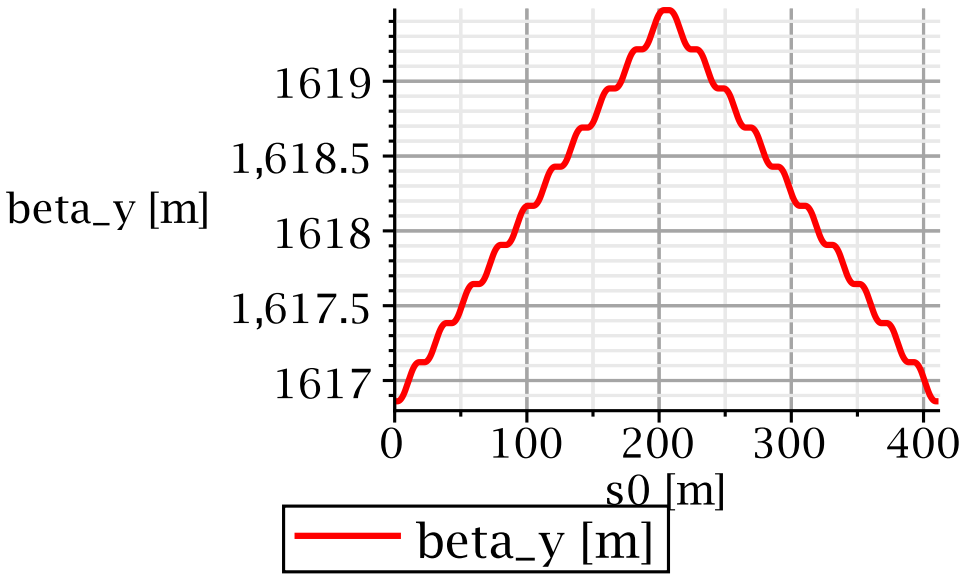

Figure 14: Vertical beta function $\beta_y(s)$, plotted for full ring. For this case the total circumference is 411.3 m and the total drift length is L_D=160.0 m. Since this total drift length exceeds $L_D^{\text{trans.}}$ as given by Eq. (27), the ring will be "below transition", as regards synchrotron oscillations.

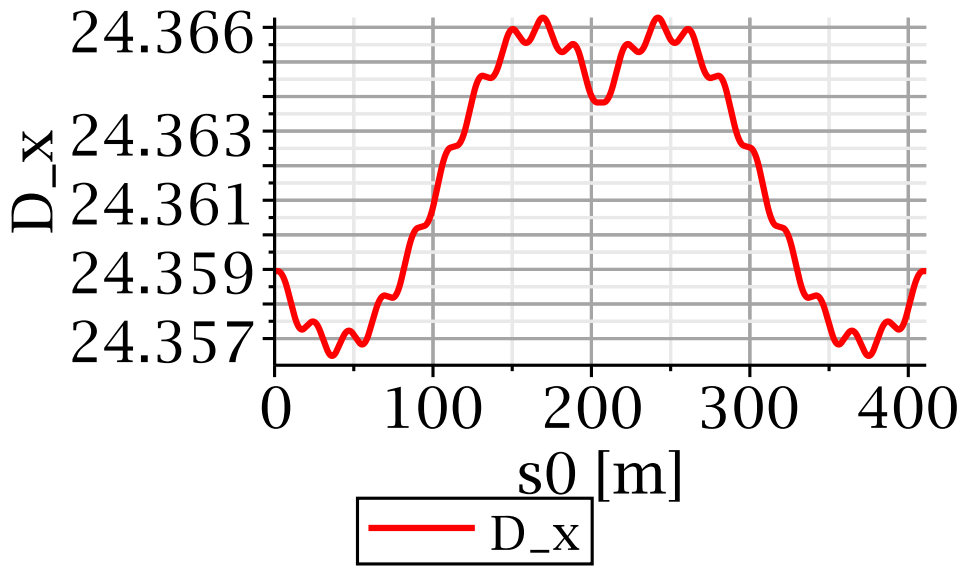

Figure 15: Outside dispersion function $D^O(s)$, plotted for full ring. For this case the total circumference is 411.3 m and the total drift length is 160.0 m. Extended decimal places exhibit the extreme uniformity.

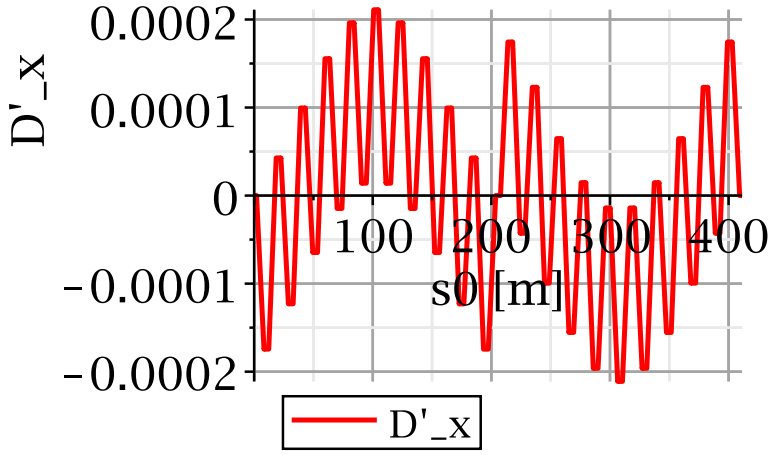

Figure 16: Outside dispersion function slope $D^O(s)'$, plotted for full ring. For this case the total circumference is 411.3 m and the total drift length is 160.0 m.

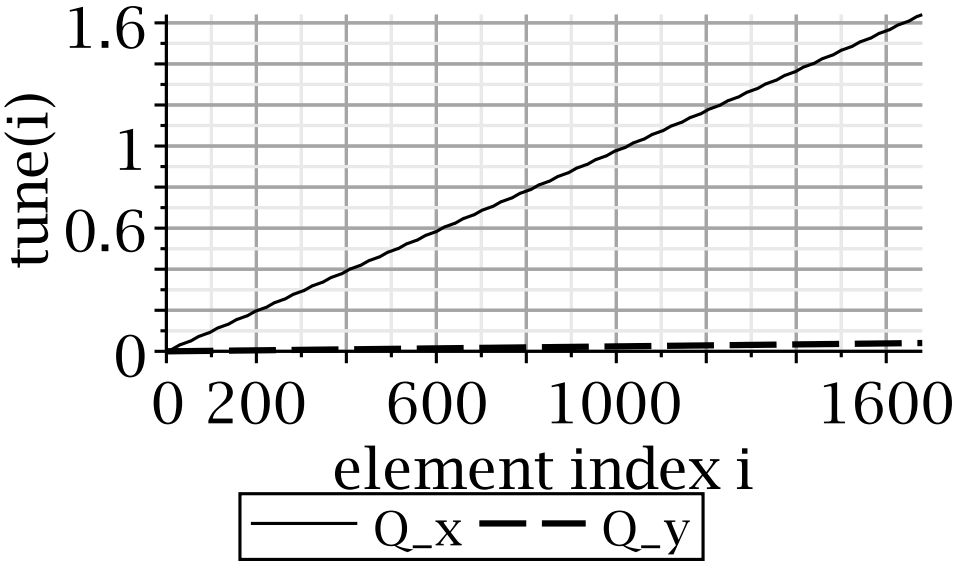

Figure 17: Transverse tune advances. The full lattice tunes are $Q_x = 1.640$ and $Q_y = 0.04046$. Evn smaller horizontal tune (for improved self-magnetometry) can be provided by trim quadrupoles. If possible, rather than by vertical electrode-contouring, the vertical field contouring will be provided electrically, and be consistent with zero quadrupole focusing, but withoctupole focusing for net vertical stability.

5 Analytic betatron oscillation description

This final section provides analytic formalas for horizontal optical functions in a lattice with constant m-value. As argued previously, because the vertical focusing is assumed to be so weak, its effect on horizontal motion is being neglected. Since the alterating gradient vertical focusing is being treated as constant vertical focusing, the field index m will be very different from the $\pm m$ alternating gradient field indices appearing in earlier sections.

For the lattice dependencies shown in the previous section, and Figure 17 in particular, the value of m has to be chosen to match the vertical tune value $Q_y = 0.04046$ given in that figure. In practice one will try to reduce Q_y from this value, even knowing that the vertical beta function will increase proportionally from the already-large value shown in Figure 14.

5.1 Differential equation "cylindrical" m=0 case

The momentum vector components are defined by

$$\mathbf{p} = p_r\hat{\mathbf{r}} + p_\theta\hat{\theta} + p_y\hat{\mathbf{y}} = \frac{m_p\dot{r}}{\sqrt{1-v^2/c^2}}\,\hat{\mathbf{r}} + \frac{m_p r\dot{\theta}}{\sqrt{1-v^2/c^2}}\,\hat{\theta} + \frac{m_p\dot{y}}{\sqrt{1-v^2/c^2}}\,\hat{\mathbf{y}}. \tag{31}$$

(Except for possible end effects) the electric force alters only the radial momentum component

$$\frac{dp_r}{dt} = -eE_0\frac{r_0}{r}. \tag{32}$$

It is important to exploit the (approximate) invariance of the system to translation along the y-axis, which causes p_y to be conserved, and to rotation around the central axis, which causes L_y, the vertical component of angular momentum, to be conserved. For a particle in the horizontal plane containing the origin the angular momentum vector is

$$\mathbf{L} = \mathbf{r}\times\mathbf{p} = -\frac{m_p r\dot{y}}{\sqrt{1-v^2/c^2}}\,\hat{\theta} + \frac{m_p r^2\dot{\theta}}{\sqrt{1-v^2/c^2}}\,\hat{\mathbf{y}} = L_\theta\hat{\theta} + L_y\hat{\mathbf{y}}. \tag{33}$$

The design orbit angular momentum is

$$L_0c/e = r_0p_0c/e \overset{\text{e.g.}}{=} 28.0\,\text{GV-m}. \tag{34}$$

We seek the orbit differential equation giving dependent variable r as a function of independent variable θ. The (conserved) total proton energy $\mathcal{E}$ is the sum of the mechanical energy and the potential energy

$$\mathcal{E} = \sqrt{p_r^2c^2 + p_\theta^2c^2 + p_y^2c^2 + m_p^2c^4} + eV(r). \tag{35}$$

Squaring this equation yields

$$\big(\mathcal{E} - eV(r)\big)^2 = p_r^2c^2 + p_\theta^2c^2 + p_y^2c^2 + m_p^2c^4. \tag{36}$$

The terms on the right hand side of this equation can be expressed in terms of r, $dr/d\theta$, and conserved quantities. From Eqs. (31) and (33),

$$p_\theta = \frac{L_y}{r}. \tag{37}$$

p_r can be expressed similarly using Eq. (11);

$$\frac{p_r}{p_\theta} = \frac{\dot{r}}{r\dot{\theta}} = \frac{1}{r}\frac{dr}{d\theta}, \quad \text{and hence} \quad p_r = \frac{L_y}{r^2}\frac{dr}{d\theta}. \tag{38}$$

Making these substitutions yields

$$\left(\mathcal{E} - eV(r)\right)^2 = \left(\frac{L_y c}{r^2}\frac{dr}{d\theta}\right)^2 + \frac{L_y^2 c^2}{r^2} + p_y^2 c^2 + m_p^2 c^4, \tag{39}$$

as the first order differential equation for orbits within bend elements.

5.2 Small deviation from the pure cylindrical case

The $m = 0$ case is singular and, as shown above, leads to a logarithmic potential. To produce weak vertical focusing the radial electric field has to fall off as $1/r^{1+m}$, where $0 < m$. This deviation from the pure cylindrical case, and the fact that the logarithmic potential is inconvenient, suggests that we proceed with a small m approximation, which becomes exact in the m=0 limit. The electric field and electric potential for y=0 are given by Eqs. (1) and (2). The independent (longitudinal) coordinate s is to be replaced by the angular coordinate,

$$\theta = \frac{s}{r_0}. \tag{40}$$

We change the dependent variable from $x(s) = r - r_0$ (with independendent variable s) to a (dimensionless) dependent variable $\xi(\theta)$ (with independendent variable θ) producing

$$x' \equiv \frac{dx}{ds}, \quad \text{and} \quad \xi' \equiv \frac{d\xi}{d\theta} \tag{41}$$

The present discussion is limited to planar orbits, in which case the definition of x by $r = r_0 + x$ is the conventional Frenet accelerator definition. Note that ξ is proportional to x for small x. For mnemonic purposes one can think of ξ (in linearized approximation) as the customary accelerator radial variable x, but measured in units of bend radius r_0. For a "large" displacement, say x=1 cm, at 40 m ring radius, the value of ξ is 2.5×10^{-4}.

For r taken to be a polar (rather than cylindrical) coordinate these definitions are not quite exact but realistic vertical amplitudes will usually be small enough that the effect on x of projection onto the horizontal plane can be neglected. The substitution

$$\frac{1}{r} = \frac{1-\xi}{r_0}, \tag{42}$$

which motivates this change of variables, will be prominent in subsequent formulas. Inverse relations are

$$x = \frac{r_0\xi}{1-\xi}, \quad \text{and} \quad x' = \frac{r_0 d\xi/ds}{(1-\xi)^2} = \frac{\xi'}{(1-\xi)^2}. \tag{43}$$

Expressed as power series in ξ, with the leading terms cancelling, the electric potential is given by Eq. (12). We are primarily interested in the small m case. In this approximation

Eq. (39) becomes

$$\left(\mathcal{E} - eE_0r_0\Big(\xi + \frac{1-m}{2}\xi^2 + \frac{(1-m)(2-m)}{6}\xi^3\Big)\right)^2 = \frac{L_y^2c^2}{r_0^2}\,\xi'^2 + \frac{L_y^2c^2}{r_0^2}\,(1-\xi)^2 + p_y^2c^2 + m_p^2c^4. \tag{44}$$

More terms in the power series expansion could be retained easily, but the term proportional to ξ^2 can be expected to dominate any nonlinearity-driven spin decoherence. By retaining just this term, without assuming $|m| << 1$, the Kepler case can also be covered. Expanding the left hand side,

$$\mathcal{E}^2 - 2\mathcal{E}eE_0r_0\xi - \mathcal{E}eE_0r_0(1-m)\xi^2 - \mathcal{E}eE_0r_0(1-m)(2-m)\xi^3 + e^2E_0^2r_0^2\xi^2 + e^2E_0^2r_0^2(1-m)\xi^3 = \frac{L_y^2c^2}{r_0^2}\,\xi'^2 + \frac{L_y^2c^2}{r_0^2}\,(1-\xi)^2 + p_y^2c^2 + m_p^2c^4. \tag{45}$$

which retains terms up to ξ^3, while retaining the validity of the equation for m=1. Differentiating this equation with respect to θ, dividing through by ξ', dropping nonlinear terms, and re-arranging the equation, produces

$$\xi'' = 1 - \frac{eE_0r_0^3\mathcal{E}}{L_y^2c^2} - \xi - \frac{eE_0r_0^3\mathcal{E}}{L_y^2c^2}(1-m)\xi + \frac{e^2E_0^2r_0^4}{L_y^2c^2}\xi. \tag{46}$$

This is the equation for offset simple harmonic motion.

As contrasted with E_0 and r_0, which are true constants, $\mathcal{E}$ and L_y are only constants of the motion, close to but not in general equal to $\mathcal{E}_0$ and L_{y0}. Also, neglecting to include a term proportional to p_y' is fully justified only for $m = 0$. Nevertheless, for simplicity, to apply linearization, we can neglect these refinements. Noting that $eE_0r_0^3\mathcal{E}_0 \approx (L_yc)^2$ and $eE_0r_0^2/(L_yc) \approx \beta$, Eq. (46) then becomes

$$\xi'' = 1 - 1 - \Big(1 + (1-m) - \beta^2\Big)\xi = -\Big(1 - m + \frac{1}{\gamma^2}\Big)\xi \tag{47}$$

This is the linearized equation of motion for on-momentum particles. A more general linearized equation, applicable off-momentum, is obtained using

$$\frac{eE_0r_0^3\mathcal{E}}{L_y^2c^2} = \frac{L_0^2}{L_y^2}\,\frac{\mathcal{E}}{\mathcal{E}_0}, \quad \text{and} \quad \frac{e^2E_0^2r_0^4}{L_y^2c^2} = \beta^2\,\frac{L_0^2}{L_y^2}. \tag{48}$$

This yields

$$\xi'' = 1 - \frac{L_0^2}{L_y^2}\,\frac{\mathcal{E}}{\mathcal{E}_0} - \left(\frac{L_0^2}{L_y^2}\,\frac{\mathcal{E}}{\mathcal{E}_0}(1-m) + 1 - \beta^2\,\frac{L_0^2}{L_y^2}\right)\xi. \tag{49}$$

6 Horizontal betatron oscillations

Restoring the leading nonlinear term, and grouping terms appropriately, the orbit equation can be abbreviated as

$$\frac{d^2\xi}{d\theta^2} = -Q^2(\xi - \xi_{\rm co}) + \frac{3}{2}\,\beta^2\,\frac{L_0^2}{L_y^2}(1-m)\xi^2, \tag{50}$$

where

$$Q^2 = 1 + \frac{L_0^2}{L_y^2}\,\frac{\mathcal{E}}{\mathcal{E}_0}(1-m) - \beta^2\,\frac{L_0^2}{L_y^2} \quad \text{and} \quad \xi_{\rm co} = \frac{1 - \frac{L_0^2}{L_y^2}\,\frac{\mathcal{E}}{\mathcal{E}_0}}{Q^2}. \tag{51}$$

After this abbreviation the equation has been reduced to simple harmonic motion, offset relative to equilibrium point $\xi_{\rm co}$, which is the ξ-value for which the linearized r.h.s. vanishes.

Some special case horizontal tune values for a homogeneous, weak-focusing, all-electric storage ring, with central (not necessarily magic) γ-value γ_0, are

$$Q_{x0}^{m=1} = \frac{1}{\gamma_0}, \quad Q_{x0}^{m=0} = \sqrt{1 + \frac{1}{\gamma_0^2}}, \quad Q_{x0}^{|m|<<1} \approx Q_{x0}^{m=0} - \frac{m/2}{Q_{x0}^{m=0}} \tag{52}$$

When tracking particle orbits in a computer program it is important to realize that the parameters in Eq. (51) need to be worked out on a particle-by-particle basis. The coefficients Q and $\xi_{\rm co}$, though approximately the same for all particles, depends on the dynamic variables $\mathcal{E}$, L_y, and β, which depend on the coordinates of the particle being tracked. This complication is too tedious for analytic formulation.

It is noteworthy that the nonlinear term vanishes in the Kepler, m=1 case. In this case the motion is said to be "integrable" and the motion remains (offset-) sinusoidal even for arbitrarily large amplitudes.

6.0.1 Tracking the full transverse oscillation amplitude

For propagating $\Delta\xi = \xi - \xi_{\rm co}$, one introduces cosine-like trajectory $C_\xi(\theta)$ satisfying $C_\xi(0) = 1$, $C'_\xi(0) = 0$ and sine-like trajectory $S_\xi(\theta)$ satisfying $S_\xi(0) = 0$, $S'_\xi(0) = 1$. They are given by

$$\begin{aligned} C_\xi(\theta) &= \cos(Q\theta) \\ C'_\xi(\theta) &= -Q\,\sin(Q\theta) \\ S_\xi(\theta) &= \frac{\sin(Q\theta)}{Q} \\ S'_\xi(\theta) &= \cos(Q\theta), \end{aligned} \tag{53}$$

where Q, as given by Eq. (52) depends on m. For our lattice in which m alternates between equal but opposite values of m, both small compared to 1, Q will be nearly independent of m for evolution over large arcs of the ring.

For describing evolution of (ξ, ξ') from its initial values $(\xi_{\rm in}, \xi'_{\rm in})$ at $\theta = 0$ to its values at θ one can use the "transfer matrix" defined by

$$\mathbf{M}_\xi\,(\theta) = \begin{pmatrix} C_\xi(\theta) & S_\xi(\theta) \\ C'_\xi(\theta) & S'_\xi(\theta) \end{pmatrix}, \tag{54}$$

to give

$$\begin{pmatrix}\xi(\theta)\\ \xi'(\theta)\end{pmatrix} = \begin{pmatrix}\xi_{\rm co}\\ \xi'_{\rm co}\end{pmatrix} + \mathbf{M}_\xi(\theta)\begin{pmatrix}\xi_{\rm in}-\xi_{\rm co}\\ \xi'_{\rm in}-\xi'_{\rm co}\end{pmatrix}. \tag{55}$$

or

$$\begin{aligned}\xi(\theta) &= \xi_{\rm co} + C_\xi(\theta)(\xi_{\rm in}-\xi_{\rm co}) + S_\xi(\theta)(\xi'_{\rm in}-\xi'_{\rm co}),\\ \xi'(\theta) &= \xi'_{\rm co} + C'_\xi(\theta)(\xi_{\rm in}-\xi_{\rm co}) + S'_\xi(\theta)(\xi'_{\rm in}-\xi'_{\rm co}).\end{aligned} \tag{56}$$

Initial conditions $(\xi_{\rm in}, \xi'_{\rm in})$ can be expressed in terms of initial x conditions;

$$\xi_{\rm in} = \frac{x_{\rm in}}{r_0 + x_{\rm in}}, \quad \xi'_{\rm in} = \frac{r_0^2 x'_{\rm in}}{(r_0 + x_{\rm in})^2}. \tag{57}$$

Substitution from Eqs. (57) into Eqs. (56) gives a description of the evolution of $(\xi(\theta), \xi'(\theta))$, from initial conditions $(x_{\rm in}, x'_{\rm in})$.

For the proton EDM experiment the value of radius r_0 will be, say, 40 m. An initial value $x_{\rm in} = 1$ m would be unrealistically large. It is better therefore to use centimeter units. Then $r_0 = 4000$ cm. With the gap width being 3 cm, a typical amplitude is 1 in these units, and (allowing for radial offset due to momentum) a maximal surviving amplitude is about 1 in these units. Even at this amplitude the nonlinear correction, for example in the denominators of Eq. (57), is only 1 part in 4000.

6.0.2 Chromaticity

For betatron oscillations relative to off-energy closed orbits it is appropriate to evaluate Q from Eq. (51). We have that, for circular orbits in the $1/r$ field, mechanical parameters within bends, such as γ^I are constant and hence cannot be used to label different circular orbits. But, as long as the closed orbits are circles they can be labeled by x or by γ^O. On these circles, assuming $m = 0$,

$$\frac{L_0}{L_{y,\rm c.o.}} = \frac{r_0 p_0}{(r_0 + D^O\delta)p_0} r_0 p_0 \approx 1 - \frac{D^O}{r_0}\,\delta. \tag{58}$$

In the definition of angular momentum as momentum times radius, the radius has gone from r_0 to $r_0 + x_0$ but the momentum has not changed. The energy ratio can be similarly expressed,

$$\frac{\mathcal{E}_0|_{x_{co}=x_0}}{\mathcal{E}_0} = 1 + \frac{eE_0x_0}{\mathcal{E}_0} \approx 1 + \frac{\Delta\gamma^O}{\gamma_0} \approx 1 + \beta_0^2\,\frac{x_0}{r_0}. \tag{59}$$

Substituting these expressions into Q^2, as given by Eq. (51), one obtains the dependence of tune on fractional momentum offset;

$$Q^2 = 1 + \left(1 - 2\frac{D^O}{r_0}\delta\right)\left(1 + \beta_0^2\,\frac{D_0}{r_0}\delta\right)(1-m) - \beta^2\left(1 - 2\frac{D^O}{r_0}\delta\right). \tag{60}$$

The full expression is left unsimplified as a reminder of the source of the expression.

6.0.3 Fast/slow, betatron/synchrotron separation

One treatment of Eq. (51) is to evaluate Q^2 and $\xi_{\rm co}$ on the design orbit and to treat them as being the same for all particles. To incorporate energy variation Q^2 and $\xi_{\rm co}$ are treated as functions of the energy offset or, more conventionally, as functions of the fractional momentum offset δ^O.

In magnetic ring this produces the standard, linearized, description of the motion as being the sum of a rapidly varying betatron part and a slowly varying synchrotron part. This separation is not very well motivated for electric lattices, since the mechanical energy of each particle varies on the betatron oscillation time scale. This invalidates the conventional betatron/synchrotron separation paradigm, at least superficially.

The general solution of Eq. (50) can be written as the sum of a general solution of the homogeneous part and a specific solution of the inhomogeneous part, where the term $Q^2\xi_{\rm co}$ on the r.h.s. is the inhomogenous term.

In spite of the locally varying speed, the homogeneous solution can be referred to as "betatron oscillation". It can also be referred to as "fast" oscillation (in spite of the fact that, for the proton EDM experiment, the betatron tune will be not much greater than 1, which would usually be reqarded as a very low tune. The inhomogeneous solution can be referred to as "synchrotron oscillation", which may also be referred to as "slow" oscillation, even though this is appropriate only *outside* bend elements.

6.0.4 Kinematic variables within electric bend elements

The electric field and electric potential are given by Eqs. (9) and (12);

$$\begin{aligned}
\mathbf{E}(\xi) &= -E_0\,(1-\xi)^{1+m}\,\hat{\mathbf{r}}, \\
V(\xi) &= E_0 r_0 \left(\xi + \frac{1-m}{2}\xi^2 + \frac{(1-m)(2-m)}{6}\xi^3 \ldots \right).
\end{aligned} \tag{61}$$

The latter equation, along with Eq. (56), permits the potential energy to be expressed in terms of θ and initial conditions, to determine the electric potential at all points on a particle orbit;.

$$V(\theta) = E_0 r_0 \left(\xi_{\rm co} + (\xi_{\rm in} - \xi_{\rm co})\,\cos Q\theta + \frac{\xi'_{\rm in}}{Q}\,\sin Q\theta + \frac{1-m}{2}\xi^2 + \frac{(1-m)(2-m)}{6}\xi^3 \ldots \right). \tag{62}$$

where the betatron oscillation substitution has been made for ξ has been made only for the linear term, but should be made also for ξ^2 and ξ^3. Though not exhibited notationally, Q depends on m, as given by Eq. (51).

Then $\gamma(\theta)$ is obtained from

$$\begin{aligned}
\gamma(\theta) = \frac{\mathcal{E}}{m_p c^2} - \frac{E_0 r_0}{m_p c^2/e} \times \\
\times \left(\xi_{\rm co} + (\xi_{\rm in} - \xi_{\rm co})\,\cos Q\theta + \frac{\xi'_{\rm in}}{Q}\,\sin Q\theta + \frac{1-m}{2}\xi^2 + \frac{(1-m)(2-m)}{6}\xi^3 \ldots \right).
\end{aligned} \tag{63}$$

From this formula one can obtain $\beta(\theta)$ using $\beta(\theta) = \sqrt{1 - 1/\gamma^2(\theta)}$. From the y-component of Eq. (33) we also have, for motion in the horizontal plane,

$$\frac{d\theta}{dt} = \frac{-L_y}{m_p r^2 \gamma}. \tag{64}$$

Note that, with right-handed Frenet coordinates, and clockwise orbit (which we are now assuming) L_y is negative. This accounts for the negative sign in Eq. (64). The right hand side of this equation can now be expressed in terms of θ, invariants and initial conditions.

Note that the sign of θ and the sign of L_y are correlated in Eq. (64). The negative sign $(-L_y)$ is specific to clockwise orbits, with θ increasing along the orbit. This sign ambiguity causes the tracked time of flight variable ct to also be ambiguous. The appropriate RF phase is then, similarly, ambiguous.

References

[1] R. and J. Talman, *Symplectic orbit and spin tracking code for all-electric storage rings,* Phys. Rev. ST Accel Beams **18**, ZD10091, 2015

[2] R. and J. Talman, *Electric Dipole Momment Planning with a resurrected BNL Alternating Gradient Synchrotron electron analog ring,* Phys. Rev. ST Accel Beams **18**, ZD10092, 2015

[3] R. Talman and J. Talman, *Octupole focusing relativistic self-magnetometer electric storage ring bottle,* arXiv:1512.00884-[physics.acc-ph], 2015

[4] C. Møller, *The Theory of Relativity,* Clarendon Press, Oxford, 1952

[5] J.D. Jackson, *Classical Electrodynamics,* 3rd edition, John Wiley, 1999

[6] G. Muñoz and I. Pavic, *A Hamilton-like vector for the special-relativistic Coulomb problem,* Eur. J. Phys. **27**, 1007-1018, 2006

[7] H.B. Dwight, *Tables of Integrals and Other Mathematical Data,* MacMillan Publishing Co., Inc., 1961